Structure and valence of the Ce/Pt(111) system

J. Tang and J. M. Lawrence
Institute for Surface and Interface Science and Department of Physics, University of California, Irvine, California 92717

J. C. Hemminger
Institute for Surface and Interface Science and Department of Chemistry, University of California, Irvine, California 92717

(Received 21 June 1993)

We have studied the growth of thin cerium films on Pt(111) with x-ray photoemission spectroscopy (XPS) and low-energy electron diffraction. No ordered structures were observed for the Ce films immediately after room-temperature deposition. After heat treatment to 770 K, ordered Ce-Pt compounds were formed. For films with initial coverages greater than 3.5 ML, a hexagonal pattern with periodicity nearly twice that of Pt(111) appeared after annealing. For this 1.96×1.96 structure, the periodicity is close to that of the compound $CePt_2$, the XPS data show a stoichiometry of $CePt_{2.23}$, and the observed Ce valence is 3.07. For films having initial coverages from 0.9 to 1.8 ML, a 1.94×1.94 pattern with small satellites around the main spots appeared; the Ce valence is 3.11 and the stoichiometry is $CePt_3$. Between 2.1 and 3.2 ML, a 1.96×1.96 pattern with a superimposed 1.96×1.96 net rotated by 30° was observed with valence around 3.09. Studies of the take-off angle dependence of the emission indicate that the valence has the same value near the surface as in the bulk. We have also performed CO and O_2 adsorption studies and found extremely low sticking coefficients for these molecules on the 1.96×1.96 $CePt_{2.23}$ surface. Since these well-characterized single-crystal Ce compound films are highly suitable for photoemission experiments and adsorption studies, we have attempted to formulate empirical rules for predicting which compound species will be generated by similar means.

I. INTRODUCTION

In the past, most heavy-fermion photoemission experiments have been performed on polycrystalline samples without careful characterization of the sample surface. Since photoemission is a surface-sensitive technique, it is extremely important to know the surface contribution.

The usual method for preparing (exposing) clean sample surfaces for these experiments has been to cleave or scrape the polycrystalline compounds in vacuum. The sample surfaces generated by these methods are difficult to characterize, either in terms of local stoichiometry or surface reconstruction. Another less commonly used method for obtaining clean sample surfaces is ion bombardment followed by annealing. For this approach the stoichiometry may deviate from the expected value due to preferential sputtering, and the structural damage done to the sample surface is usually unknown.

It has been shown for polycrystalline samples of mixed-valent $CeIr_2$ that the cerium at the sample surface is trivalent.[1] Similarly the surface of Sm is divalent, while the bulk is trivalent.[2] (The convention in the study of rare-earth mixed-valence compounds is that the valence is the number of $5d6s$ conduction electrons per atom that contribute to the bonding. For cerium the valence z is related to the $4f$ occupation number n_f via $z=4-n_f$.) On the other hand, in the Ce/W(110) system[3] the cerium is known to change from γ-like to α-like at the surface as the first Ce monolayer increases its packing density. (By "γ-like" we mean weakly mixed valent, comparable to γ-Ce where the valence is $z=3.05$ and the f count is $n_f=0.95$; by "α-like" we mean comparable to strongly mixed-valent materials such as α-Ce or $CeIr_2$ where $z=3.25$ and $n_f=0.75$.) Clearly the surface cerium electronic state is sensitive to structure so that its behavior at a single-crystal compound surface cannot be simply predicted.

Besides these problems, distortion of the spectra by contaminants is also significant. While contamination from residual gases in the chamber can be controlled by improving the vacuum, for polycrystalline samples another source of contamination arises: the contaminants can hide along the grain boundaries and migrate to the sample surface after cleaving or scraping. The degree of this source of contamination depends in an unknown way on the compound species. In the case where migration is rapid, data must be collected rapidly, which limits the statistics of the spectra.

There have been several studies involving rare-earth films deposited on transition-metal surfaces, such as Nd/Cu(111),[4] Yb/Cu(100),[5] Sm/Cu(111)[6] and Eu/Pd(111),[7] where ordered compound(s) were observed and/or identified after annealing. In this work, we attempt to grow single-crystal cerium intermetallics by evaporating clean cerium films onto clean Pt(111) substrates and annealing *in situ*. We use low-energy electron diffraction (LEED) to determine structure and XPS (with varying take-off angle) to determine surface and bulk stoichiometry and valence. (The Ce $3d$ core level is used to measure the valence.) Our major objective is to learn how to grow clean, well-characterized single-crystal Ce intermetallics for use in future heavy-fermion photoemis-

sion experiments and for adsorbate chemistry studies. We also compare these results for the Ce/Pt(111) system to our previous results for Ce on Pt foils[8] where room-temperature intermixing between the freshly deposited Ce and the foil substrate was emphasized.

II. EXPERIMENT

The experiments were performed in a VG ESCALAB MKII system equipped with a preparation chamber that has a 6-in. reverse view LEED apparatus from Princeton Research Instruments and a Ce evaporator installed. The base pressure was 6×10^{-11} mbar, and the operation pressure was 1×10^{-10} mbar. The aluminum $K\alpha$ x-ray source and hemispherical analyzer provide overall resolution for XPS of 1 eV. The ultraviolet photoemission spectra (UPS) were obtained using a differentially pumped He lamp; the chamber pressure during the UPS data collection was 4×10^{-10} mbar. The Pt(111) substrate was cleaned by cycles of argon sputtering followed by annealing in the presence of oxygen. The possible bulk contaminants (Ca, C, and S) were all monitored by XPS. No Ca or S was found, and the C level was less than 0.5% after these cleaning procedures. The annealing was achieved by resistively heating a Re wire surrounding the crystal; temperatures of 1600 K can be achieved. The Ce film cleanliness was also monitored by XPS, the oxygen level being less than 1.5% of a monolayer. The Pt substrate was cleaned in a separate chamber from the Ce evaporation chamber so that oxygen treatment of the Pt would not affect the Ce cleanliness. Other details regarding Ce cleanliness and contaminant effects are discussed in our earlier report.[8] A pin-hole directional doser was used for the O_2 and CO adsorption studies, where the equivalent exposure was calibrated by CO/Pt(111) uptake experiments. For the studies of annealed Ce films we usually heated the samples at 770 K for 5 min; occasionally we followed this by further annealing at higher temperatures and/or for longer time intervals. Our system (especially the sample manipulator and heating path) was thoroughly degassed before these experiments so that the chamber pressure during annealing was always around 1×10^{-10} mbar.

The LEED periodicities were determined by measuring the distance between spots on the LEED photographs. We estimate the error from this procedure to be 1%.

The Ce $3d$ and Pt $4f$ core-level XPS provide information about the coverage, Ce valence, stoichiometry, and structure. The spectra of the Pt $4d$ core level were also used for coverage information. The C and O regions were recorded to check for cleanliness and for the absorption studies. Emission for both normal and large take-off angles were recorded, where the "large take-off angle" (LTA) was 80° from the sample normal. In order to perform quantitative analysis, it is important to determine the XPS sensitivity factors of Ce and Pt. We have measured the absolute count rates for the pure substances under the same photoemission conditions (x-ray flux, sample position, emission angle, etc.). The Ce to Pt sensitivity factor ratio we obtained is 2.38, which is very close to the number obtained from an identical VG instrument.[9]

We have used a simple layer-by-layer growth model, which was described in our earlier report,[8] to convert the XPS Ce-Pt intensity ratio before annealing into Ce coverages. The Pt $4d$ region was also used to provide coverage information through the following equation:

$$\frac{I_{[\mathrm{Pt}\ 4f]}}{I_{[\mathrm{Pt}\ 4d]}}=\alpha\exp(-d/\lambda_{4f})/\exp(-d/\lambda_{4d}),$$

where α is a constant related to the $4f$ and $4d$ ionization crosssections, d is the film thickness, and the λ's are the respective mean free paths for Pt $4d$ and Pt $4f$ electrons. The mean free paths are obtained from the universal curve for electron escape depth vs kinetic energy.[10] The values of coverage obtained were comparable (to within 20%) to those obtained from the Ce_{3d}-Pt_{4f} ratios.

The measured stoichiometries for the annealing compounds (Table I) are determined from the Ce-Pt intensity ratios using experimentally measured sensitivity factors, under the assumption that the compound is homogeneous within the probing depth. Possible sources of error are first that the sensitivity factors may not be directly applicable in the compound (due to differences in the atomic arrangements) and second that the compound may not be homogeneous, but may exhibit a stoichiometry gradient.

III. RESULTS AND ANALYSIS

In this section, the terminologies "trivalent," mixed-valent, "α-like," "γ-like," and "f-count (n_f)" will be used as defined above. As explained in our previous paper,[8] we are less interested in precise values of the valence than in trends; therefore, such qualitative description of the valence should be adequate for our purpose. The valence is obtained from the Ce $3d$ spectra in standard fashion;[8,11,12] essentially we determine the relative weight of the emission due to the f^0 state (at 915 eV) to emission from the f^1 state (at 902–903 eV) and the f^2 state (at $\sim$897 eV). All binding-energy values are obtained from our data after performing background subtraction and curve fitting to the spectra. We discuss the results obtained prior to annealing first; then we discuss the annealed, ordered films.

A. Before annealing

No ordered Ce structures were observed by LEED immediately after the room-temperature deposition of Ce. At lower coverages (<0.9 ML), the Pt(111) LEED pattern became fuzzy; at higher coverages, no Pt(111) LEED pattern was observed.

Figure 1 shows normal-emission Ce $3d$ spectra before annealing; the curves at lower coverages are magnified to provide better comparison. At the coverage 0.2 ML, the Ce is trivalent. Mixed valent behavior can first be observed at the coverage 0.3 ML; it becomes strongest between 1.2 and 1.5 ML where the line shapes resemble that of α-Ce. As the coverage increases, the line shape becomes close to that of γ-cerium.

In Fig. 2 we show the Pt $4f$ spectra corresponding to those in Fig. 1. The $4f$ binding energy gradually shifts towards a larger value as the coverage increases. The difference in the Pt $4f$ binding energy between the clean

Pt substrate and the highly converged substrate is 0.5 eV.

A plot of the measured Ce $3d_{3/2}$ binding energy is presented in Fig. 3. The value for γ-Ce that was measured in our system is indicated for comparison. The binding energy decreases towards the γ-Ce value as the coverage increases.

In Fig. 4 the Ce $3d$ spectra for normal emission and for large take-off angle (LTA) emission are compared: In (a), the Ce coverage is 0.3 ML; there is no significant difference between the upper and lower curves. In (b), the Ce coverage is 1.2 ML; both curves show mixed-valent features, but the upper curve has slightly lower $4f^0$ height at 915 eV. In (c), the coverage is 2.7 ML; the overall mixed valence has reduced, and the upper curve still shows a smaller $4f^0$ peak. In (d), the Ce coverage is 5.4 ML; the two curves are similar again, but here the features are both close to that of γ cerium.

Table I lists the Ce-Pt intensity ratios measured for normal and LTA emission for different coverages before annealing, and the corresponding stoichiometries and valences after annealing. We do not estimate stoichiometry for the unannealed films as the Ce-Pt ratios are averaged within the probing depth and do not necessarily imply homogeneous structures.

B. After annealing

In the following, the term "coverage" will refer to the coverage prior to annealing, and the LEED patterns will be referenced to the Pt(111) lattice unit, so that "1.96×1.96" represents a structure with periodicity 1.96 times that of the Pt "1×1" structure.

We found four surface structure, depending on coverage (Fig. 5). For the lowest coverages ($\theta<0.7$ ML) the LEED pattern after annealing is that of Pt(111). The $3d$ line shape does not change significantly after annealing, so that the Ce has γ-like (weak) mixed valence (Table I).

For coverages in the range $0.9<\theta<1.8$ ML the LEED pattern shows main spots with nearly 2×2 periodicity (it varies from 1.94×1.94 at the lower coverages to

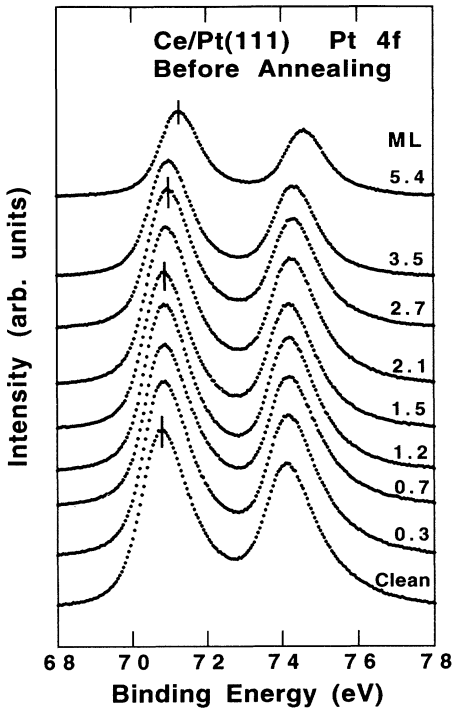

FIG. 2. The Pt $4f$ XPS prior to annealing. As the coverage increases the $4f$ binding energy increases. The net shift from the clean substrate to the 5.4-ML film is 0.5 eV.

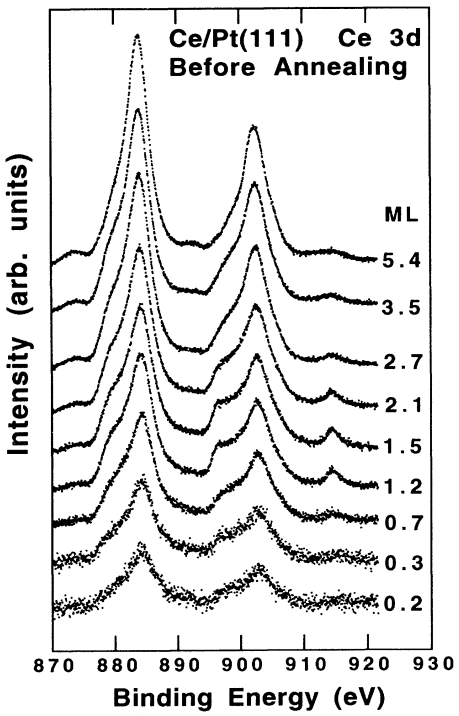

FIG. 1. The Ce $3d$ XPS for as-deposited Ce/Pt(111) films prior to annealing as a function of coverage. The line shape indicates that the Ce is trivalent at 0.2 ML; at 0.3 ML weak mixed valence occurs. From 1.2 to 1.5 ML, the mixed-valent feature is strongest. Above 2.7 ML the mixed valence weakens and resembles that of γ-Ce.

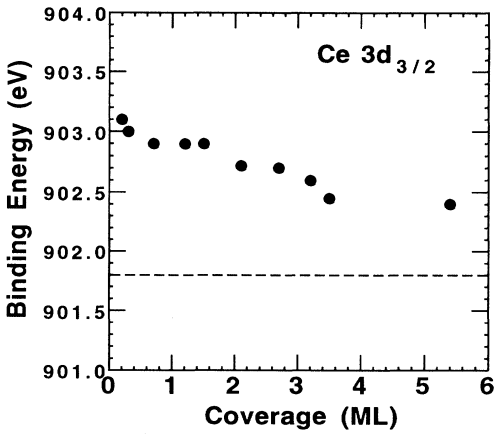

FIG. 3. The Ce $3d_{3/2}$ binding energy as a function of coverage for the unannealed film. The binding energy decreases as the coverage increases; the shift from 0.2 to 5.4 ML is 0.7 eV. The value for γ-cerium is indicated by the dashed line.

1.96×1.96 at the higher) with a hexagonal pattern of lower intensity satellites surrounding the main spots [Fig. 6(a)]. These satellites represent a superstructure whose periodicity is 5.2 times that of the 1.94×1.94 structure. Occasionally a larger net of outer satellite can be resolved. (This pattern is sometimes observed for coverages as low as $\theta=0.7$ ML.) The Ce valence for this structure is of order 3.11 [Fig. 7(c) and Table I].

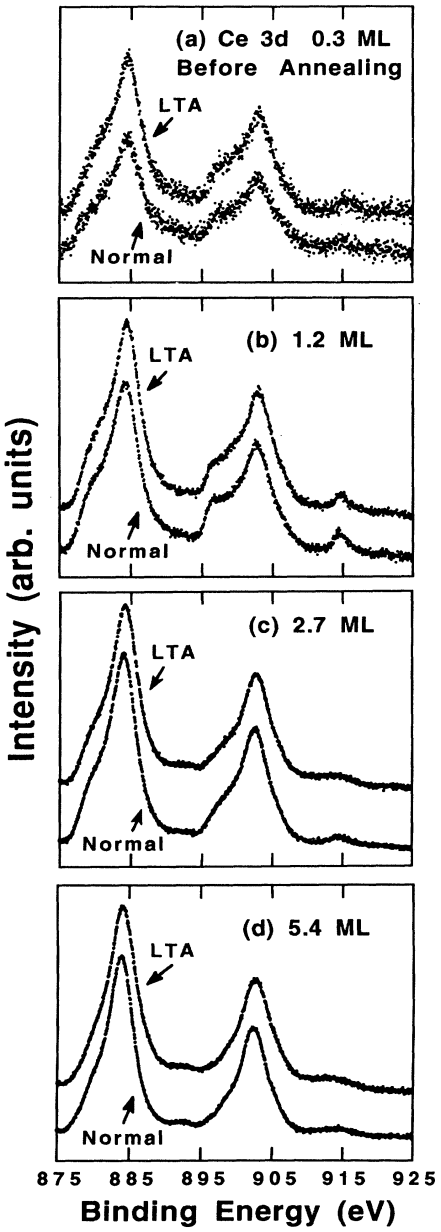

FIG. 4. Comparison for the unannealed films of Ce 3*d* XPS between large take-off angle (LTA) and normal emission. The coverages displayed are 0.3, 1.2, 2.7, and 5.4 ML. At 0.3 ML the line shapes are similar. At 1.2 and 2.7 ML the LTA line shapes have slightly lower $4f^0$ peaks at 915 eV than those for normal emission. At 5.4 ML both line shapes are similar; the Ce is weakly mixed valent. The existence of a large $4f^0$ peak at 1.2 ML represents a strong Ce-Pt interaction.

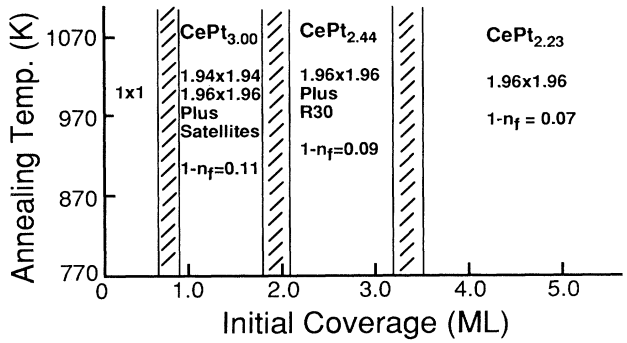

FIG. 5. Phase diagram of the annealed Ce/Pt(111) system. Below 0.7 ML (the area marked "1×1"), only LEED patterns corresponding to Pt(111) were observed. The Ce-Pt stoichiometries, LEED patterns, and Ce valences are indicated for other regions. From 0.9 to 1.8 ML, 1.94×1.94 (0.9–1.2 ML) or 1.96×1.96 (1.5–1.8 ML)-plus-satellite LEED patterns appear. From 2.1 to 3.2 ML a 1.96×1.96 plus *R*30 pattern is seen in LEED; since the stoichiometry and Ce valence change gradually, the numbers displayed are for 2.7 ML. Above 3.5 ML only one LEED pattern (1.96×1.96) and Ce valence are observed. The stoichiometries and valences for different coverages are also included in Table I.

For coverages $2.1<\theta<3.2$ ML the LEED pattern [Fig. 6(b)] shows a 1.96×1.96 pattern plus a superimposed net rotated by 30°; the periodicity for the "*R*30" structure is the same as that of the main 1.96×1.96 pattern, within measurement error. As can be seen from Fig. 7(b) and Table I, the Ce valence for this structure (3.09) is somewhat smaller than in the satellite structure seen at lower coverages.

For coverages above 3.5 ML the LEED pattern [Fig. 6(c)] is that of a simple hexagonal 1.96×1.96 structure (without satellites or rotated nets of spots). The valence is 3.07 [Fig. 7(c) and Table I].

When spectra at large take-off angle are compared to normal-emission spectra (Fig. 7) it is found that the 3*d* line shape does not vary with take-off angle in any of the three ordered structures. This means that the valence is the same near the surface as in the bulk of the ordered compound. Furthermore, examination of Table I shows another important feature: the Ce/Pt ratio is always smaller for large take-off angle, implying that the surface region is Pt rich (except for very low coverages in the 1×1 region of Fig. 5).

The phase diagram of Fig. 5 summarizes these structures. The boundaries are not exact, in part due to the limited number of coverages studied. The upper and lower limits of each region were set equal to the highest or lowest coverage where each distinct LEED pattern was observed. The temperature range represent the range of annealing temperatures that we utilized. The stoichiometries for the different structures deduced from Ce-Pt peak area ratios are given in Fig. 5 and Table II.

C. Adsorption studies

Figures 8 and 9 show the results from CO and O_2 adsorption studies on the annealed 1.96×1.96 Ce-Pt com-

TABLE I. The stoichiometries measured from normal and large take-off angle (LTA) emission before and after annealing for different initial Ce coverages. The Ce valence after annealing is also listed. The stoichiometry calculation is based on the measured Ce-Pt XPS sensitivity ratio 2.38.

Coverage (ML)	Before annealing Ce-Pt ratio normal	Before annealing Ce-Pt ratio LTA	After annealing Ce-Pt ratio normal	After annealing Ce-Pt ratio LTA	After annealing Stoichiometry normal	After annealing Stoichiometry LTA	Cerium valence
0.3	0.17	0.38	0.10	0.22	$Ce_{0.04}Pt_{0.96}$	$Ce_{0.08}Pt_{0.92}$	3.08
0.7	0.45	0.92	0.19	0.36	$Ce_{0.07}Pt_{0.93}$	$Ce_{0.13}Pt_{0.87}$	3.09
1.2	0.91	1.34	0.81	0.52	$Ce_{0.25}Pt_{0.75}$	$Ce_{0.18}Pt_{0.82}$	3.12
1.5	1.10	1.66	0.80	0.47	$Ce_{0.25}Pt_{0.75}$	$Ce_{0.16}Pt_{0.84}$	3.11
2.1	1.52	2.55	0.95	0.63	$Ce_{0.28}Pt_{0.72}$	$Ce_{0.21}Pt_{0.79}$	3.09
2.7	2.00	3.47	1.00	0.61	$Ce_{0.29}Pt_{0.71}$	$Ce_{0.20}Pt_{0.80}$	3.08
3.5	3.02	3.81	1.04	0.7	$Ce_{0.30}Pt_{0.70}$	$Ce_{0.23}Pt_{0.77}$	3.07
5.4	5.2	6.45	1.07	0.63	$Ce_{0.31}Pt_{0.69}$	$Ce_{0.22}Pt_{0.78}$	3.07

pound surface (the initial coverage is 5.0 ML). In Fig. 8(a) the Ce 3*d* region before and after dosage with 200 langmuirs (1 L$=10^{-6}$ torr s) of CO is displayed; in Fig. 8(b) the C 1*s* region is displayed. The increase in the C 1*s* signal corresponds to a C uptake of only 7% of a monolayer. The sticking coefficient is therefore less than 0.001. The O_2 adsorption results in Fig. 9 shows an increase of the oxygen 1*s* peak area which corresponds to an uptake of only 4% of a monolayer for an O_2 exposure of 200 L. The O_2 sticking coefficient is also less than 0.001.

IV. DISCUSSION

A. As-deposited films

In earlier studies[8] of the growth of Ce films on polycrystalline Pt, Ir, and Re foils we concluded that Ce films on Re grow without interdiffusion or reaction with the substrate, but Ce/Pt films deposited at room temperature exhibit substantial intermixing (i.e., interdiffusion and Ce/Pt reaction). The evidence for these conclusions was drawn from comparison of trends in the Ce 3*d* binding energy, in the degree of mixed valence, and in the Pt 4*f* binding energy as coverage increased, as well as from the effect of annealing on the Ce 3*d* spectra. The present results (Figs. 1–4, Table I) for Ce films as deposited on Pt(111) at room temperature extend the earlier results to a single-crystal surface and to higher coverages (5.4 versus 2.55 ML) and include the feature that we have studied the take-off angle dependence of the emission. We note that following points of comparison.

First, the Pt 4*f* binding energy shifts continuously with coverage in identical fashion but to an even larger value (0.5 eV at 5.4 ML) than in the earlier work (0.2 eV at 2.55 ML) due to the higher coverage. This shift gives evidence that the Pt interacts strongly with the Ce. (For Ce/Re where no intermixing occurs, no Re 4*f* shift is observed.)

TABLE II. Space-group symmetry and the Gibbs free energy of formation for Sm-Cu and Ce-Pt compounds. The Sm-Cu values are obtained from Ref. 21, and the Ce-Pt values are from Refs. 22 and 23. The temperature dependence (i.e., ΔS) of the Gibbs free energy for CePt is not known, but a reasonable estimate of 0.05 K J/mol for ΔS can be obtained by inspecting values for the rest of the available lanthanide-Pt compounds in Ref. 22.

Compound	Space group	ΔG_f (570 K) K J/mol	ΔG_f (670 K) K J/mol	ΔG_f (770 K) K J/mol
		Sm-Cu Compounds		
Cu	$Fm\bar{3}m$			
$SmCu_6$	*Pnma*	−22.13	−21.01	−20.04
$SmCu_5$	*P6/mmm*	−30.64	−28.44	−26.24
$SmCu_4$	*Pnnm*	−25.66	−24.64	−23.63
$SmCu_2$	*Imma*	−27.25	−26.82	−26.40
SmCu	$Pm\bar{3}m$	−30.89	−29.42	−27.94

Compound	Space group	ΔG_f (770 K) K J/mol	ΔG_f (870 K) K J/mol	ΔG_f (970 K) K J/mol
		Ce-Pt Compounds		
Pt	$Fm\bar{3}m$			
$CePt_5$	*P6/mmm*	−79.73	−78.77	−75.89
$CePt_2$	$Fd\bar{3}m$	−179.33	−176.23	−166.93
CePt	*Cmcm*	−74.40	−69.40	−54.40

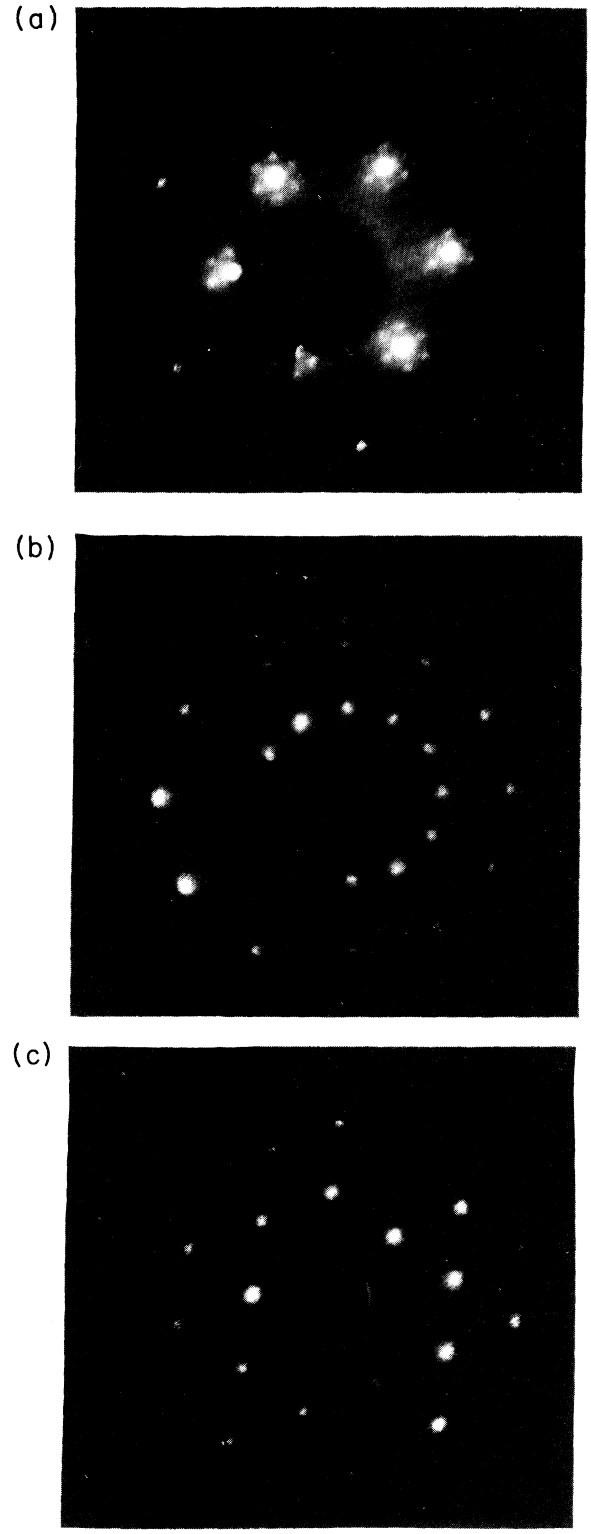

FIG. 6. LEED patterns observed after annealing at different coverages (annealing temperature 770 K): (a) At 1.5 ML the main pattern is 1.96×1.96; the small satellites correspond to a periodicity that is 5.2 times the main compound periodicity. (b) At 2.7 ML, there is a 1.96×1.96 pattern plus a superimposed $R30$ pattern which has the same 1.96×1.96 periodicity. (c) At 5.4 ML, only a simple 1.96×1.96 pattern exists.

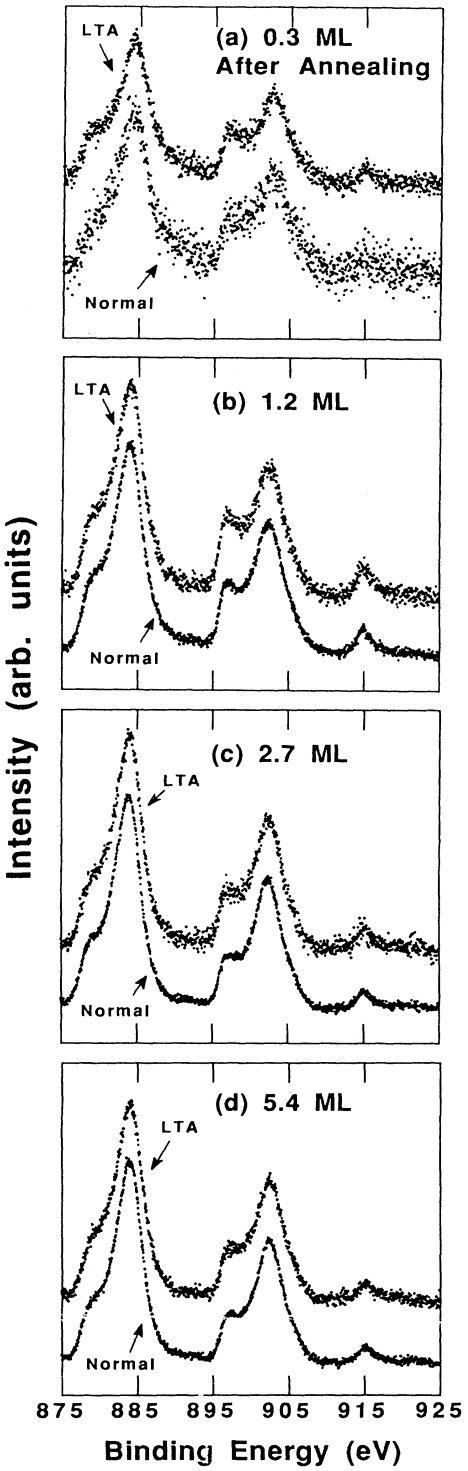

FIG. 7. Comparison for annealed films of the Ce $3d$ XPS line shapes between large take-off angle (LTA) and normal emission for the coverages 0.3, 1.2, 2.7, and 5.4 ML. The LTA spectra are normalized to those taken at normal emission. The difference in line shape between the upper and lower curves in all four panels is small. The signal-to-noise ratio in the LTA curves is smaller, because the Ce population is small due to the small probing depth and because the signal sits on top of a background of secondary electrons.

The Ce $3d_{3/2}$ binding energy at low converge [903.1 eV for Ce/Pt(111); 903.5 eV for Ce/Pt (poly)] has approximately the same value for Ce/Re and Ce/Ir; the value appears to be characteristic of an isolated poorly screened Ce atom adsorbed on the surface of the M substrate. As the coverage increases the $3d_{3/2}$ energy approaches the γ-Ce value very slowly compared to the Ce/Re case, where a γ-Ce film is already formed at 2 ML. This gives further support for intermixing in the Ce/Pt system.

The cerium is trivalent at the lowest coverage; the threshold for the onset of mixed valence is lower (0.3 ML) for Ce/Pt(111) than for Ce/Pt(poly) (0.5 ML). The valence increases steadily out to approximately 1.5 ML (Fig. 1), as in the earlier work;[8] the Ce-Pt intermixing causes fairly strong (α-like) mixed valence. At higher coverages of order 5 ML the valence (as well as the $3d_{3/2}$ binding energy) approaches the value expected for γ-Ce. This gives evidence (not observable at the lower coverages studied in the older work[8]) that for these coverages an unreacted γ-like layer begins to form on top of the Ce-Pt mixed layer. Consistent with this, the studies of the take-off angle dependence of the $3d$ line shape (Fig. 4) show for the higher coverages ($\theta > 1$ ML) that the valence at the surface is always smaller, or more nearly γ-like, than in the bulk. At the same time, the stoichiometry (or Ce/Pt ratio) is always Ce rich near the surface (Table I). Clearly there is a gradient, or gradual increase of the Pt concentration, on going from the surface into the bulk; for thicker films the γ-Ce surface layer will occupy most of the XPS probing depth.

In summary, the present results are fully consistent

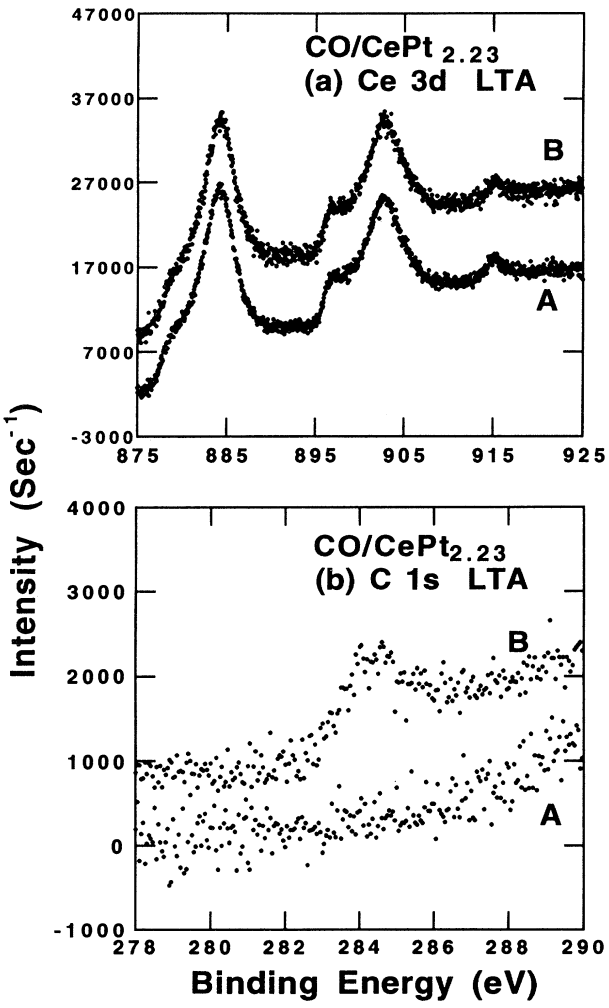

FIG. 8. XPS spectra before and after dosing $CePt_{2.23}$ (initial coverage 5.0 ML; LEED pattern 1.96×1.96) with 200 L of CO, and measured at large take-off angles to enhance surface sensitivity. In the upper panel the Ce $3d$ region is exhibited; there is no observable change following exposure to CO. In the lower panel the C $1s$ region is shown; the increase in the C $1s$ signal corresponds to an uptake of less than 7% of a monolayer and a sticking coefficient of 0.000 35.

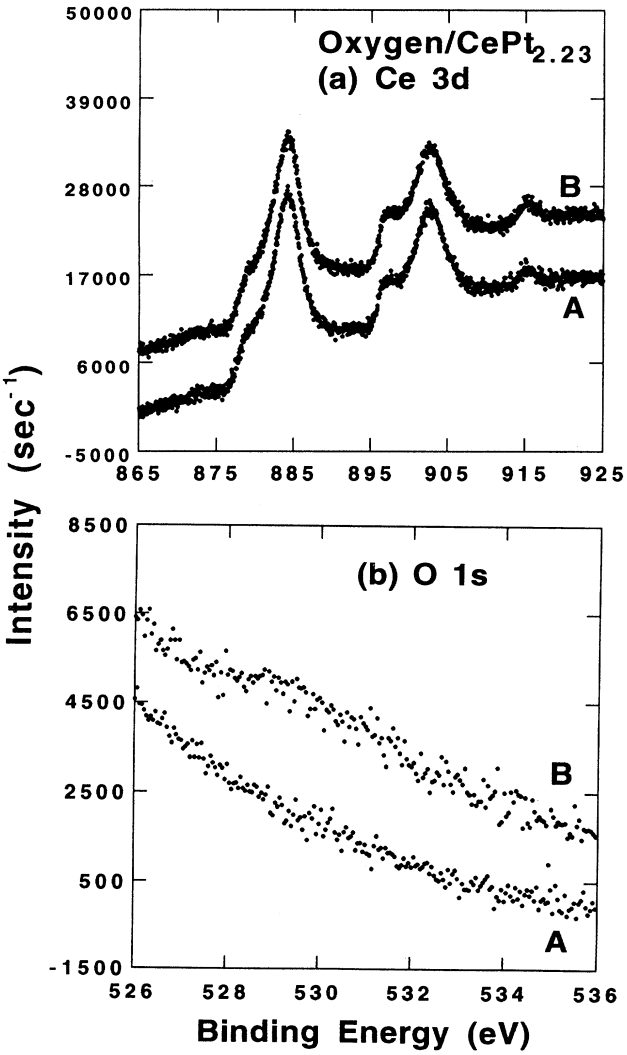

FIG. 9. XPS results for O_2 adsorption studies. Upper panel: the Ce $3d$ large take-off angle emission before and after dosing with 200 L of O_2; the line shape does not change significantly. Lower panel: the corresponding O $1s$ region; the change in the O $1s$ emission represents 4% of a monolayer at the surface, and a sticking coefficient of 0.0002.

with the earlier work (with minor differences probably due to use of a single-crystal face, rather than a polycrystalline average) showing substantial intermixing at room temperature. They further extend these studies to higher coverages where growth of a γ-cerium layer on top of the mixed layer becomes apparent.

B. Structures of the annealed films

Examination of Table I shows that for films with initial coverages $1<\theta<5$ ML annealing creates ordered structures with stoichiometries varying continuously between $CePt_3$ and $CePt_2$. Hence we consider first the known crystal structures of the bulk compounds.[13,14] The $C15$ Laves phase compound $CePt_2$ has a cubic unit cell containing 8 Ce and 16 Pt atoms. Six layers of triangular nets stack along the (111) direction to form this structure; the alternating layers 1, 3, and 5 consist of pure Pt, the other layers (2, 4, and 6) mix Ce and Pt in an overall 2:1 ratio.[13] Both the symmetry (triangular nets) and lattice constant ($a_0=7.71$ Å) are amenable for 2×2 growth on Pt, where $2a_0=7.84$ Å.[15] This structure has an extensive range of stoichiometry, so that single phase samples of $CePt_{2+x}$ can be grown for $0\le x\le1$, with lattice constant varying linearly with x to the value 7.65 Å for $CePt_3$.[14] (A small amount of splitting of certain reflections was observed in x-ray-diffraction patterns of $CePt_3$, indicating a slight distortion of the cubic structure.) The $CePt_3$ structure probably forms by replacement of one-fourth of the Ce atoms by Pt atoms. The bulk properties (specific heat and susceptibility) of $CePt_2$ indicate that the Ce is trivalent;[16] but XPS and bremsstrahlung isochromat spectroscopy[12] studies of $CePt_3$ indicate that it is a mixed-valent compound ($z=3.1-3.2$). Presumably the valence varies continuously from $z=3$ to this value as x increases from 0 to 1.

1. Low coverges $\theta\le0.7$ ML

At low coverages only Pt(111) spots are observed in LEED. The Ce/Pt ratio decreases after annealing suggesting that a substantial fraction of the Ce migrates deeper than the XPS probing depth. The stoichiometry for large take-off angle emission is more Ce rich than for normal emission; hence there is a Ce concentration gradient with a higher Ce density near the surface. This holds even when the sample is annealed above 1070 K, suggesting that the surface structure is stable and further diffusion of the Ce into the bulk is not favorable.

While the structure could be a random surface alloy, the existence of small ordered regions cannot be ruled out; as long as the distortion of the Pt crystal structure is not large, the Pt(111) spots will still be observed in LEED. Such short-range order should be related to the ordered phases at higher coverage. Consistent with this, we note that the surface valence at $\theta=0.3$ ML is larger after annealing, and comparable to that observed after annealing higher coverage films (Figs. 4 and 7).

2. Intermediate coverages $0.9<\theta<1.8$ ML

For these coverages the stoichiometry measured at normal emission ($Ce_{0.25}Pt_{0.75}$) is that of $CePt_3$. The LEED pattern is nearly 2×2 (1.94×1.94 at $\theta=1.2$ ML; 1.96×1.96 at $\theta=1.5$ ML) with a hexagonal net of satellites. The basic periodicity is very close to the value [1.95 a_0 (Pt)] expected for $CePt_3$. The $3d$ XPS (Fig. 7) indicates strong mixed valence, as seen in the $3d$ XPS of bulk $CePt_3$ compounds.[12]

The hexagonal net of satellites represents a superstructure with a real-space periodicity 5.2 times that of the compound [and hence 10.2 times that of Pt(111)]. This superstructure may arise to relieve the stress due to the lattice mismatch (2–3%) between the thin ordered intermetallic and the underlying Pt(111) surface. Alternately, the satellites may be related to the above-mentioned distortion of the cubic cell which may occur in $CePt_3$.

A very interesting feature of this structure is that the surface stoichiometry, as measured via large take-off angle emission, is Pt rich ($Ce_{0.16}Pt_{0.84}$) relative to the normal-emission stoichiometry. In the $C15$ structure this could arise if the outermost layer was one of the layers (1, 3, or 5 as discussed above) consisting entirely of Pt. Since the probing depth is low for LTA emission the outermost layer would dominate the stoichiometry. This could also explain the interesting fact that the Ce valence is identical for LTA and normal emission: the Ce would first occur in the second layer, so that its valence would be that of the bulk compound, rather than being trivalent as expected for Ce on the outer surface.[1] (Of course, we cannot rule out that there is additional segregation of Pt to the surface over and beyond that expected in the $C15$ structure.)

Comparison to as-deposited films at these coverages brings out two interesting features: Annealing has much less effect on the (normal-emission) Ce-Pt ratio than for the other coverages (Table I); and it has very little effect on the Ce valence (Figs. 4 and 7). This suggests that the as-deposited films may consist of a mixed layer of polycrystalline $CePt_3$; the effect of annealing would then be to increase the crystallite size, without substantial diffusion of Ce atoms deeper into the bulk.

3. Intermediate coverages $1.8\le\theta\le3.2$ ML

For these coverages LEED shows a 1.96×1.96 hexagonal pattern plus an $R30$ net of the same periodicity. The intensity of these $R30$ spots depends somewhat on initial coverage and on the position of the electron beam on the sample. The stoichiometry varies from $Ce_{0.27}Pt_{0.73}$ at 1.8 ML to $Ce_{0.29}Pt_{0.71}$ at 2.7 ML and the mixed valence is a bit weaker than in the lower coverage ($CePt_3$) regime. As for the $CePt_3$ case the surface is Pt rich (Table I) and the valence is identical for LTA and normal emission. A possible explanation of this structure is that it consists of two sets of domains of $CePt_{2+x}$ (with possibly different values of x in the two domains, but with average stoichiometry $x=0.45-0.55$) oriented by 30° with respect to each other; this structure may represent an alternate mode for relieving the lattice mismatch to Pt(111).

Comparison of the Ce-Pt ratio for normal emission at these coverages before and after annealing (Table I) sug-

gests that substantial migration of Ce, beyond the XPS probing depth, is promoted by annealing. The valence varies from that of a γ-like film before annealing [Fig. 4(c)] to a moderately mixed valent in the 1.96×1.96 $R30$ structure, as would be expected if a cerium-rich film was converted to an ordered $CePt_{2+x}$ intermetallic.

4. *High coverages $\theta > 3.5$ ML*

For these coverages the LEED pattern has a simple hexagonal 1.96×1.96 structure. The normal-emission stoichiometry $Ce_{0.31}Pt_{0.69}$ is equivalent to $CePt_{2+x}$ with $x=0.23$. The films are moderately mixed valent (Fig. 7); and as for the other structures, the surface is Pt rich relative to the bulk and the valence is the same for surface-sensitive LTA emission as for bulk-sensitive normal emission.

These results are consistent with the formation of a $CePt_{2+x}$ compound with $x=0.23$. This value of x is also consistent with the fact that the measured valence (3.07) is intermediate between that $CePt_2$ ($z=3.0$) and of $CePt_3$ ($z=3.12$) and with the fact that the measured periodicity (1.96×1.96) is intermediate between that expected for $CePt_2$ (1.97×1.97) and that expected for $CePt_3$ (1.95×1.95).

Annealing causes a fivefold reduction in the Ce-Pt count rate ratio (Table I) and a strong increase in the degree of mixed valence (Figs. 4 and 7). This suggests diffusion of Ce well into the bulk and formation of a thick $CePt_{2+x}$ layer. However, additional annealing (over and above the initial 5-min anneal at 770 K) both for longer intervals (up to 2 h) at 770 K or at temperatures up to 1070 K caused no further changes in the Ce-Pt ratio, the LEED pattern, or the valence. Apparently, once the $CePt_{2+x}$ compound forms, further interdiffusion is inhibited.

C. Adsorption studies

Our CO and O_2 adsorption studies on the 1.96×1.96 $CePt_{2.23}$ substrate indicate that the sticking coefficient for these molecules is very low at room temperature: the very small increases in C 1*s* or O 1*s* count rates (Figs. 8 and 9) for exposures of more than 200 L indicate sticking coefficients less than or equal to 0.001 for both molecules. This is an extremely surprising result, not only because both molecules do adsorb on Pt(111) but also because formation of cerium oxides occurs readily in most Ce compounds.

In transition metals the partially delocalized *d* electrons are believed to play the main role in molecular adsorption.[17] In Au, where the *d* band is full, CO has an extremely low sticking coefficient. To test whether a similar mechanism is valid for $CePt_{2.23}$ we have measured the valence-band photoemission spectra (Fig. 10) at photon energies $h\nu=21.2$ and 40.8 eV. The Pt 5*d* emission dominates at the lower photon energy; it certainly does not suggest a filled *d* band, for which a corelike level should appear several eV below the Fermi level.

Clearly the low sticking coefficients cannot be explained by this mechanism. The fact that the outer layer

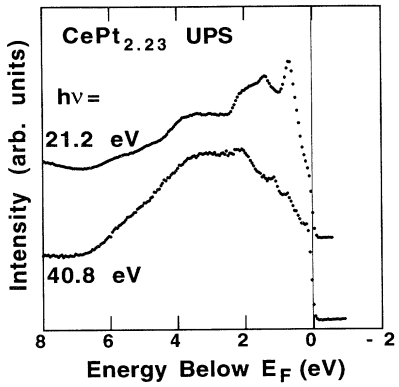

FIG. 10. He I (21.2 eV) and He II (40.8 eV) UPS for the compound $CePt_{2.23}$ (initial coverage 5.0 ML). The sharp peak that appears 0.6 eV below the Fermi level in the He I curve has a strong photon energy dependence and may correspond to a surface state (see Ref. 17). The key point is that the Pt *d* band does not appear to be filled.

of the *C*15 structure consists purely of Pt atoms may be relevant. Possibly, the moderately strong Ce mixed valence may play a role; alternately, the low adsorption may be a property of RPt_{2+x} compounds that is not unique to Ce (e.g., it may hold in $LaPt_{2+x}$). Further adsorption studies, such as on La/Pt(11) or on Ce/*M* systems with other transition metals (e.g., $M=$Pd) with varying degrees of mixed valence will be necessary to understand this phenomenon.

At higher temperatures oxidation does occur. Figure 11 shows the effect on the Ce 3*d* line shapes of exposure

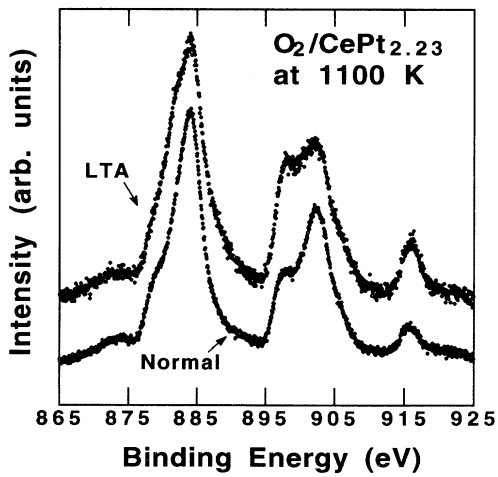

FIG. 11. Changes in the Ce 3*d* XPS (taken for large take-off angle and normal emission) after exposure of $CePt_{2.23}$ to approximately 10 L of oxygen at high temperature (1070 K). (From O 1*s* measurements the ratio of O atoms to Ce atoms was found to be 0.38.) The LTA emission indicates growth of Ce oxide in the surface region; the normal-emission spectra are very similar to that of the clean $CePt_{2.23}$ films, indicating that oxidation occurs primarily in the surface region. (These curves also demonstrate the sensitivity of Ce 3*d* XPS to differences between surface and bulk structures.)

of the $CePt_{2.23}$ surface to approximately 10 L oxygen at 1070 K. While the effect on the bulk-sensitive normal-emission spectrum is small, there is a drastic change in the LTA emission spectrum. The latter spectrum represents a mixture of Ce oxide[18] and Ce-Pt compound. (Measurements of the O 1*s* level show that the ratio of the number of oxygen atoms to the number of cerium atoms is 0.38.)

D. General comments

1. The valence of Ce at the surface

Our results for the annealed films show no significant difference in the valence between bulk-sensitive normal-emission spectra and surface-sensitive LTA emission spectra, for any of the coverages reported here (Fig. 7). These results contrast distinctly with those of Ref. 1 where polycrystalline surfaces of the strongly mixed-valent compounds $CeIr_2$, $CeRh_3$, and $CePd_3$ were shown to be essentially trivalent. (We point out that our take-off angle studies are highly sensitive to changes in 3*d* line shape, and hence valence, when they occur; this can be seen clearly in Fig. 11.) For the Ce/Pt(111) case our explanation of the identity of surface and bulk valence is that the crystal surface appears to consist purely of Pt, as is possible in the $C15$ structure; the Ce is present in the second layer, but this already possesses the bulk valence. Since the results of Ref. 3 show that Ce on the W(110) surface can be strongly mixed valent, we conclude that there is no general rule stating that Ce will be trivalent at a surface.

For these reasons we feel that surface and bulk contributions to photoemission spectra need to be determined experimentally for each compound, by studies of the take-off angle and/or photon energy dependence of the spectra.[1] Attempts to infer the surface contribution without such direct experimental confirmation (e.g., Ref. 19) are not well justified.

2. Determination of Kondo temperature

We have demonstrated the ability to grow well-characterized crystalline $CePt_{2+x}$ films with several features (low CO and O_2 adsorption; equality of bulk and near-surface valence) which make them ideal candidates for studies of heavy-fermion valence-band photoemission. A potential problem is that the stoichiometry is not precisely $CePt_2$, but rather $CePt_{2+x}$ (with $x=0.23$) so that some degree of site disorder must occur. For the purposes of heavy-fermion photoemission this problem will not be too severe if the Kondo temperature (T_K) of the films can be measured independently of the valence-band photoemission experiments, since the theory predicts that kT_K is the important energy scale for the low-energy and low-temperature phenomena. Clearly an important future experiment will be to determine T_K. This can be accomplished by measuring $n_f(T)$ by studying the temperature dependence of the Ce 3*d* line shape; the curve should show a maximum derivative dn_f/dT at a temperature of order T_K.

3. Empirical rules for growth or single-crystal intermetallics

In order to grow well-characterized, single-crystal Ce intermetallic films for heavy-fermion photoemission or adsorbate studies we need empirical rules that can predict which compounds will be generated by annealing a rare-earth film deposited on a single-crystal transition-metal substrate.

In the Eu/Pd(111) system,[7] a 2×2 compound structure was observed after annealing a thick Eu film from 800 to 1000 K; the compound was characterized by XPS and x-ray diffraction to be $EuPd_3$. In the Sm/Cu(111) system,[6] the LEED pattern and Sm-Cu Auger ratio of a 4-ML Sm film changed as the annealing temperature was raised; the terminal compound was determined to be $SmCu_5$. In the Nd/Cu(111) (Ref. 4) and Nd/Cu(100) (Ref. 20) systems, $NdCu_5$ was generated after annealing a thick Nd film to high temperature.

From these studies and our present results for Ce/Pt(111) we infer the following: First of all, at low coverage the species (stoichiometry) of the intermetallic compound can depend on the initial coverage; but at higher coverage the resulting compound species will be independent of coverage (at the same annealing temperature). Second, the symmetry (space group) and orientation of the resulting compound has to be closely related to the symmetry of the substrate [for example, on a fcc(111) substrate, compounds with sixfold or threefold symmetry along the (111) direction can be generated, but not compounds with fourfold symmetry]. Third, for related reasons the lattice mismatch between the rare-earth compound and the substrate should be small (where "small" is not yet well quantified). However, for thicker compounds if the mismatch is not too serious, it can be healed at the interface layers and a stable compound can be grown on top of the mismatch region. Fourth, annealing will tend to generate the most stable compounds, i.e., those that have the highest free energy of formation.

Clearly interdiffusion is an important aspect of the growth process; the annealing temperature must be high enough to overcome local diffusion barriers. If the free energy of compound formation is large enough, the compound will form and further diffusion will be inhibited. Under other circumstances, a substantial concentration gradient might result. Furthermore, when two potential compounds have the same free energy of formation, the *R-M* concentration gradient should favor irreversible diffusion such that the compound with the higher concentration of *M* atoms should be favored. We do not understand the details of the diffusion process very well, although it is known[8,18] that rare-earth/transition-metal interdiffusion is strongest in Cu and Au, strong in Pt, somewhat weaker in Ir, and nonexistent in Re.

In the following we take the Ce/Pt(111), Sm/Cu(111), Nd/Cu(111), Nd/Cu(100), and Eu/Pd(111) systems as examples to test these rules. To this end we show in Table II the experimental free energy of formation and the space groups for all the Ce-Pt and Sm-Cu compounds. The Gibbs free energy of formation is $\Delta G_f=\Delta H-T\Delta S$, where the enthalpy ΔH and the entropy ΔS are taken

from experiments.[21–23].

For the Ce/Pt(111) system, we have listed the CePt, $CePt_2$, and $CePt_5$ compounds; experimental data for $CePt_{2.23}$ are not available. The temperature dependence of the free energy of formation in the CePt compound is missing, but can be estimated by making the reasonable approximation[22] that $\Delta S = 50$ J/mol K. The only compounds that have symmetry close to the Pt ($Fm\bar{3}m$) symmetry are $CePt_2$ ($Fd\bar{3}m$) and $CePt_5$ ($P6/mmm$). Since the free energy of formation at 770 K (i.e., at the temperature used in our studies) of $CePt_2$ is much larger than that of $CePt_5$, it follows that $CePt_2$ should be generated. As discussed above, the lattice mismatch between a_0 ($CePt_2$) and $2a_0$(Pt) is only 2%, which also favors growth of this structure. In the $CePt_{2+x}$ system where all stoichiometries $0 < x < 1$ are allowed in essentially the same crystal structure,[14] the variation of the free energy of formation with x is not known; but clearly its value for $CePt_{2.23}$ should be similar to that of $CePt_2$, since x is small.

In the Sm/Cu(111) case, only the SmCu and $SmCu_5$ compounds are possible by symmetry. These two compounds both have high free energy of formation at 570 K, so both can exist after annealing at 570 K.[6] The SmCu species is activated first at 570 K; at 670 K both species can be seen in the LEED pattern. As the temperature is raised further, only SmCu[5] is observed. Presumably this occurs due to the rule stated earlier: since the free energies of formation of SmCu and $SmCu_5$ are comparable, high-temperature diffusion should favor the compound with the highest Cu concentration.

In the Nd/Cu(111) and Nd/Cu(100) cases, the selection of product compound is simple because $NdCu_5$ ($P6/mmm$) is the only intermetallic that has symmetry appropriate for the Cu substrate. (In addition to this compound a weak 8×8 LEED structure was observed, which was explained as growth of $NdCu_2$ at the surface of $NdCu_5$; our empirical rules cannot predict such subtleties.)

In interpreting the growth of these single-crystal compounds, binary phase diagrams can be useful when the supporting experimental data on the thermodynamics are incomplete. It is generally true that the intermetallic compound that has the highest congruent melting point is the most stable compound. (For example, $CePt_2$ is the most stable Ce-Pt compound known in terms of free energy of formation and it also has the highest congruent melting point[24] 2500 K.) In the Eu/Pd(111) system, both $EuPd_2$ ($Fd\bar{3}m$) and $EuPd_3$ ($Fm\bar{3}m$) are possible candidates by symmetry. Thermodynamic measurements are not complete, but according to the Eu-Pd binary phase diagram,[24] $EuPd_3$ has the highest congruent melting point (around 1700 K), so it should be the most stable compound. Indeed, in the Eu/Pd(111) system, the compound $EuPd_3$ is grown on annealing thick Eu films.

ACKNOWLEDGMENTS

The authors thank Mr. Joel Calhoun of the Rare Earth Information Center at Ames National Laboratory for providing the free energies of formation of rare-earth compounds. This work was supported by funds from the Research Corporation (Award Number R-164) and by the Institute for Surface and Interface Science at UCI.

[1]C. Laubschat, E. Weschke, C. Holtz, M. Domke, O. Strebel, and G. Kaindl, Phys. Rev. Lett. **65**, 1639 (1990).

[2]A. Stenborg, O. Björneholm, A. Nilsson, N. Mårtensson, J. N. Andersen, and C. Wigren, Phys. Rev. B **40**, 5916 (1989).

[3]C. Gu, X. Wu, C. G. Olson, and D. W. Lynch, Phys. Rev. Lett. **67**, 1622 (1991).

[4]R. M. Nix, R. W. Judd, and R. M. Lambert, Surf. Sci. **203**, 307 (1988).

[5]J. N. Andersen, J. Onsgaard, A. Nilsson, B. Erikson, and N. Mårtensson, Surf. Sci. **202**, 183 (1988).

[6]D. M. Jaffey, A. J. Gellman, and R. Lambert, Surf. Sci. **214**, 407 (1989).

[7]F. Bertran, T. Gourieux, G. Krill, M. F. Ravet-Krill, M. Alnot, J. J. Ehrhardt, and W. Felsh, Phys. Rev. B **46**, 7829 (1992).

[8]J. Tang, J. M. Lawrence, and J. C. Hemminger, Phys. Rev. B **47**, 16477 (1993).

[9]C. S. Hemminger, T. A. Land, A. Christie, and J. C. Hemminger, Surf. Interface Anal. **15**, 323 (1990), and (private communication).

[10]See A. Zangwill, *Physics at Surfaces* (Cambridge University Press, Cambridge, 1988), p. 21.

[11]J. C. Fuggle, F. U. Hillebrecht, Z. Zolnierek, R. Lasser, Ch. Freiburg, O. Gunnarsson, and K. Schonhammer, Phys. Rev. B **27**, 7330 (1983).

[12]M. Campanga and F. U. Hillebrecht, in *Handbook on the Physics and Chemistry of Rare Earths,* edited by K. A. Gshneidner, Jr., L. Eyring, and S. Hufner (North-Holland, New York, 1987), Vol. 10, Chap. 63; D. W. Lynch and J. H. Weaver, *ibid.* Chap. 66; F. U. Hillebrecht and M. Campagna *ibid.*, Chap. 67.

[13]J. V. Smith, in *Geometrical and Structural Crystallography* (Wiley, New York, 1982), pp. 177–179.

[14]I. R. Harris, J. Less-Common Metals **14**, 459 (1968).

[15]B. D. Cullity, in *Elements of X-ray Diffraction,* 2nd ed. (Addison-Wesley, Reading, MA, 1978).

[16]R. R. Joseph, K. A. Gschneidner, Jr., and R. E. Hungsberg, Phys. Rev. B **5**, 1878 (1972).

[17]S. G. Louis, in *Physics of Transition Metals 1980,* edited by P. Rhodes (Institute of Physics, Bristol, 1981), p. 401.

[18]N. A. Braaten, J. K. Grapsted, and S. Raaen, Phys. Rev. B **40**, 7969 (1989).

[19]L. Z. Liu, J. W. Allen, O. Gunnarsson, N. E. Christensen, and O. K. Anderson, Phys. Rev. B **45**, 8934 (1992).

[20]R. M. Nix and R. M. Lambert, Surf. Sci. **186**, 163 (1987).

[21]P. R. Subramanian and D. E. Lauglin, Bull. Alloy Phase Diagrams **9**, 382 (1988).

[22]G. Kemmler (unpublished).

[23]B. M. Mogutnov and L. A. Shvartsman, Zh. Fiz. Khim. **54**, 568 (1980) [Russ. J. Phys. Chem. **54**, 328 (1980)].

[24]See, e.g., W. G. Moffatt, *The Handbook of Binary Phase Diagram* (Genium, New York, 1984), sections for related compounds.

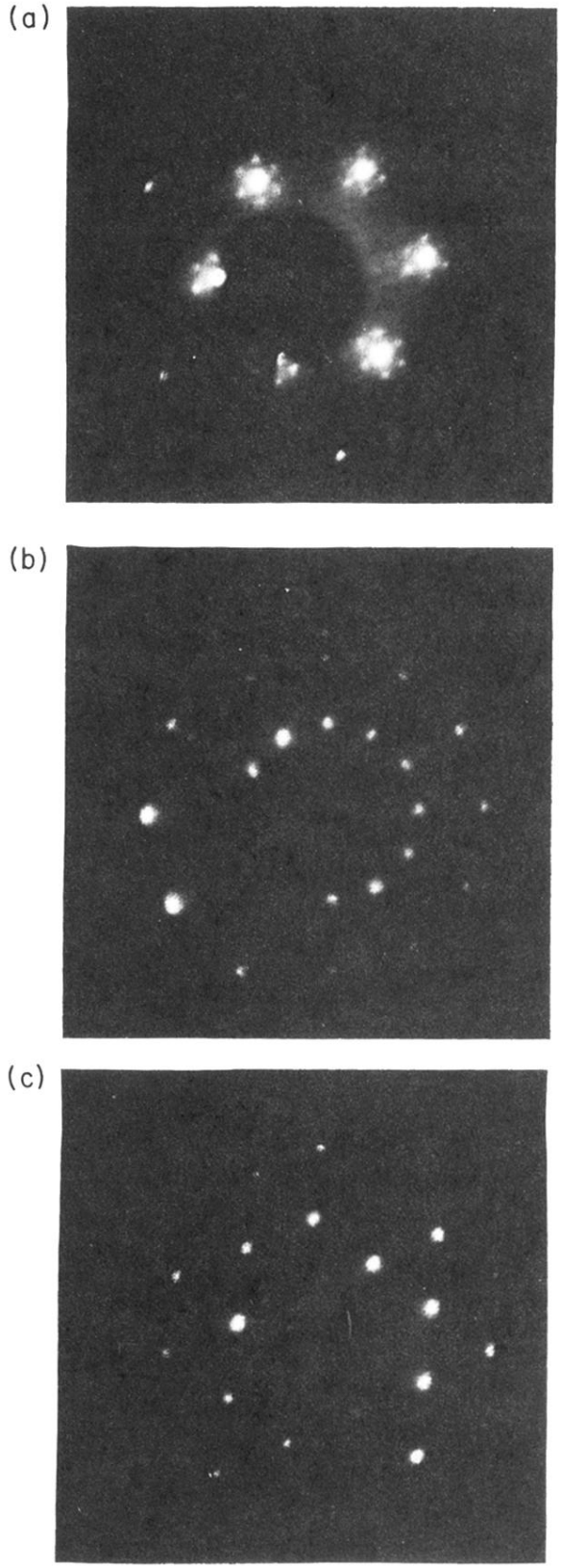

FIG. 6. LEED patterns observed after annealing at different coverages (annealing temperature 770 K): (a) At 1.5 ML the main pattern is 1.96×1.96; the small satellites correspond to a periodicity that is 5.2 times the main compound periodicity. (b) At 2.7 ML, there is a 1.96×1.96 pattern plus a superimposed $R30$ pattern which has the same 1.96×1.96 periodicity. (c) At 5.4 ML, only a simple 1.96×1.96 pattern exists.